AIAA JOURNAL
Vol. 40, No. 2, February 2002

Predictions of Transitional Flows in Low-Pressure Turbines Using Intermittency Transport Equation

Y. B. Suzen*
University of Kentucky, Lexington, Kentucky 40506-0108
G. Xiong†
Network Appliance, Inc., Sunnyvale, California 94089
and
P. G. Huang‡
University of Kentucky, Lexington, Kentucky 40506-0108

A transport equation for the intermittency factor is employed to predict the transitional flows in low-pressure turbine applications. The intermittent behavior of the transitional flows is taken into account and incorporated into computations by modifying the eddy viscosity μ_t with the intermittency factor γ. Turbulence quantities are predicted by using Menter's shear stress transport two-equation turbulence model, and the intermittency factor is obtained from the solution of a recently developed transport equation model. The transport equation model not only can reproduce the experimentally observed streamwise variation of the intermittency in the transition zone, but it also provides a realistic cross-stream variation of the intermittency profile. The current model is applied to predictions of a modern low-pressure turbine experiment, and detailed comparisons of the computational results with the experimental data are presented. The model has been shown to be capable of predicting the low-pressure turbine flow transition under a variety of Reynolds number and freestream turbulence conditions.

Nomenclature

C_p = pressure coefficient, $2(p_{\text{total}} - p)/\rho U_{\text{exit}}^2$
c_f = skin friction
K_t = flow acceleration parameter, $(\nu/U^2)(\mathrm{d}U/\mathrm{d}s)$
k = turbulence kinetic energy
L_{ss} = suction surface length
L_x = axial chord length
N = nondimensional spot breakdown rate parameter, $n\sigma\theta_{\text{t}}^3/\nu$
n = spot generation rate
p = static pressure
p_{total} = total pressure
Re = Reynolds number, $L_{\text{ss}}U_{\text{exit}}/\nu$
Re_{st} = $(s_t - s_s)U_e/\nu$
$Re_{\theta t}$ = $\theta_t U_e/\nu$
s = distance along suction surface
Tu = turbulence intensity, u'/U, %
U = boundary-layer streamwise velocity
U_e = freestream velocity
U_{exit} = exit velocity
U_{in} = inlet velocity
u_τ = friction velocity
W = magnitude of vorticity
y_n = distance normal to the wall
y^+ = $y_n u_\tau/\nu$
γ = intermittency factor
θ = momentum thickness
λ_θ = pressure gradient parameter, $(\theta^2/\nu)(\mathrm{d}U/\mathrm{d}s)$
μ = molecular viscosity
μ_t = eddy viscosity
ν = μ/ρ
ν_t = μ_t/ρ
ρ = density
σ = spot propagation parameter

Subscripts

e = freestream
s = onset of separation
t = onset of transition

I. Introduction

THE majority of flows in low-pressure turbine applications involve flow transition under the strong influences of freestream turbulence and Reynolds number effects. A thorough understanding of the underlying physics and accurate prediction of this type of complex flows are important elements in the analysis of turbine blades, in the performance evaluation of turbines, and, ultimately, in the design of jet engines.

Several methods have been proposed for the prediction of transitional flows. One approach is to make use of "pure" turbulence models. This method relies on the low-Reynolds-number modifications of turbulence models to predict transition. The studies by Savill[1,2] and Westin and Henkes[3] showed, however, that none of the available turbulence models could predict both the transition location and transition length accurately under diverse flow conditions.

Another approach for modeling transitional flows is to incorporate the concept of intermittency into computations. This can be accomplished either by using conditioned-averaged Navier–Stokes equations (see Refs. 4 and 5) or by multiplying the eddy viscosity μ_t, used in the diffusive parts of the mean flow equations, by the intermittency factor γ (Ref. 6). The former method requires the solution of two sets of highly coupled conditioned Navier–Stokes equations. Hence, this method is computationally expensive and is not compatible with the current computational fluid dynamics (CFD) methodologies. The latter approach modifies the eddy viscosity μ_t, obtained from a turbulence model, with the intermittency factor γ. That is, a modified eddy viscosity, $\mu_t^* = \gamma\mu_t$, is used in the mean flow equations. In this approach, the intermittency factor γ can be obtained

Presented as Paper 2000-2654 at Fluids 2000, Denver, CO, 19–22 June 2000; received 7 August 2000; revision received 22 March 2001; accepted for publication 25 July 2001.

*Senior Engineer Associate, Department of Mechanical Engineering. Member AIAA.
†Mechanical Engineer, Advanced Platform Packaging. Member AIAA.
‡Associate Professor, Department of Mechanical Engineering. Senior Member AIAA.

from an empirical relation such as the correlation of Dhawan and Narasimha,[7] or it can be obtained from a transport model.

Huang and Xiong[8] implemented the latter approach into the TURCOM code of Huang and Coakley[9] and successfully simulated the flows over a modern low-pressure turbine blade corresponding to the experiments of Simon et al.[10] In their computations, turbulence quantities were obtained from the shear stress transport (SST) two-equation model of Menter[11] and the streamwise intermittency distribution was prescribed by the Dhawan and Narasimha[7] correlation

$$\gamma = \begin{cases} 1 - \exp\left[-(x - x_t)^2 n\sigma / U\right] & (x \geq x_t) \\ 0 & (x < x_t) \end{cases} \tag{1}$$

where U is the freestream velocity, x_t is the point of transition onset, n is the turbulent spot formation rate, and σ is the turbulent spot propagation parameter. Note that the correlation of Dhawan and Narasimha[7] is a good representation of streamwise intermittency distribution. However, it does not provide any information about the variation of intermittency in the cross-stream direction.

In the current research, we concentrate on the prediction of transitional flows in low-pressure turbine applications by using a recently developed transport model for intermittency.[12,13] The main motivation in the development of this model is to predict flow transition under the influences of freestream turbulence and Reynolds number effects. The model can reproduce the intermittency distribution of Dhawan and Narasimha[7] in the streamwise direction and is also able to provide a proper variation of γ in the cross-stream direction. Details of the development of the model and the validation of its predicting capabilities against the T3 series experiments of Savill[1,2] are given by Suzen and Huang.[12,13] To further demonstrate the ability of the current model in predicting transitional flows, we focus on calculations of the recent experiment of Simon et al.[10] conducted at the University of Minnesota (referred to as UMN data hereafter). In the experiment, two-dimensional flows over a simulated, modern turbine blade were studied. The experiments covered a range of flow conditions including Reynolds numbers varying from 5×10^4 to 3×10^5 and freestream turbulence intensities ranging from 0.5 to 10%.

In the next section some of the flow physics and the key features of the experiment will be discussed. Section II illustrates how the Reynolds number and freestream turbulence affect the onset and the length of flow transition and how transition can affect the size of the separation bubble on the suction surface of the turbine blade. In Sec. III, details of the intermittency transport model and its implementation are described along with the empirical correlations employed for the onset of transition. The numerical details of the calculations used to predict the turbine experiments are illustrated in Sec. IV. Section V shows comparisons of the numerical predictions and the experimental data of Simon et al.[10] for a number of experimental flow conditions. These comparisons demonstrate the capability of the current intermittency approach in predicting low-pressure turbine flows under a range of flow conditions. Finally, conclusions are provided in Sec. VI.

II. Experimental Observation: The Complex Interplay Between Flow Separation and Transition

The experiment of Simon et al.[10] was performed to address the need for improved performance of low-pressure turbines by means of a better understanding of flow separation and transition. The experimental setup is shown in Fig. 1, where a simulated, modern low-pressure turbine blade (Pratt and Whitney's Pak-B blade) is studied. Measurements were made on the suction surface of the blade at locations from P2 to P13, as shown in Fig. 2, and their exact positions in terms of the suction surface length are as follows: location 2, 4.5%; location 3, 17.8%; location 4, 29%; location 5, 35%; location 6, 40.9%; location 7, 47%; location 8, 52.9%; location 9, 59%; location 10, 67.9%; location 11, 73.8%; location 12, 82.1%; and location 13, 92.6%.

The results were reported for Reynolds numbers Re (based on the exit velocity and length of the suction surface, which is about 1.8 times the Reynolds number defined by the inlet freestream velocity and suction surface length) ranging from 5×10^4 to 3×10^5 and for freestream turbulence intensity (FSTI) of the approaching flow varying from 0.5 to 10%. Table 1 summarizes some of the key experimental results that demonstrate the complex interplay among Reynolds number, freestream turbulence, flow separation, and transition. The horizontal and vertical downward directions of Table 1 are in the increasing Reynolds number and turbulence intensity directions, respectively. For each pair of Reynolds number and FSTI, the first value in Table 1 indicates the location of transition onset on the suction surface of the blade, the second value denotes the position of the onset of flow separation, and the third value shows the approximate size of the separation zone. For all Reynolds numbers and freestream turbulence intensity values Simon et al.[10] studied, the boundary layer is essentially laminar from the leading edge up to the midspan of the suction surface. As the Reynolds number and/or FSTI increases, the onset of transition moves upstream. Strong adverse

Table 1 Effects of Reynolds number and FSTI on flow separation and transition, compiled from UMN data[10]

	Reynolds number Re			
Flow	5×10^4	1×10^5	2×10^5	3×10^5
	FSTI = 0.5%			
Onset of transition[a]	79.7%	72.6%	69.4%	53.7%
Onset of separation[a]	50.3%	51.6%	54.2%	54.9%
Length of separation[b]	no reattachment	52.8%	25.6%	17.9%
	FSTI = 2.5%			
Onset of transition	67.0%	67.9%	54.6%	53.7%
Onset of separation	53.6%	53.8%	55.2%	55.2%
Length of separation	37.8%	26.8%	16.3%	12.9%
	FSTI = 10%			
Onset of transition	61.6%	56.4%	53.7%	——
Onset of separation	54.9%	55.6%	56.2%	——
Length of separation	29.2%	20.6%	12.9%	——

[a]Indicated by the relative location on the suction surface s/L_{SS}.
[b]Scaled by the suction surface length L_{SS}.

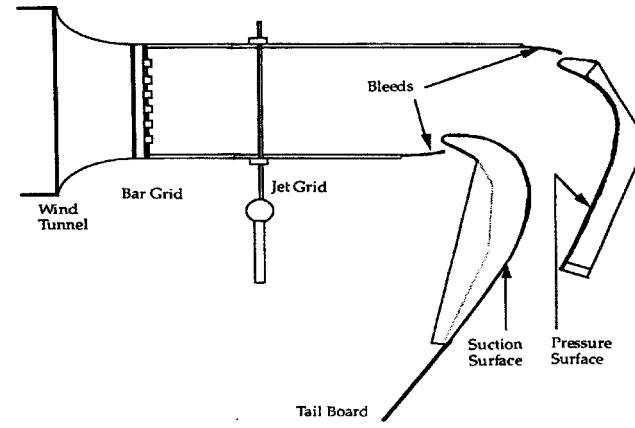

Fig. 1 Experiment setup (Simon et al.[10]): test rig.

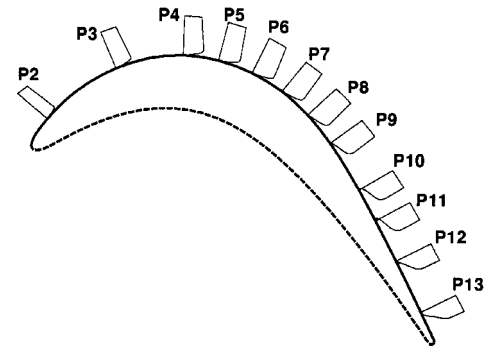

Fig. 2 Experiment setup[10]: measured stations on the suction surface of the blade.

pressure gradients downstream of the throat region of the wind tunnel cause deceleration of the flow and, hence, promote flow separation. If the flow separates in the laminar region, transition may take place in the free shear layer over the separation bubble. Transition to turbulence enhances the momentum transport in the near-wall region and eventually leads to shortening of the separation bubble. In some other circumstances, bypass transition may be observed before flow separation due to elevated FSTI coupled with the high Reynolds number of the approaching flow. This early transition would reduce the separation zone and sometimes could prevent flow separation entirely. According to UMN data, separation was observed in all cases based on surface shear stress visualization with corroboration from measured velocity profiles. In particular, for the two cases with highest Reynolds number and turbulence intensity ($Re = 2 \times 10^4$ and FSTI = 10% and $Re = 3 \times 10^5$ and FSTI = 2.5%), even though transition moved farther ahead, separation did occur. Nevertheless, partly because of the transition taking place before separation and partly due to the shortening of transition length caused by the strong adverse pressure gradient of the throat region, the separation bubble was suppressed to a very short and thin region. For these two cases, although the measured velocity profiles indicated no separation, surface visualizations showed a short separation bubble in both cases. An observation based only on the measured velocity profiles, suggesting that no separation bubble exists for the two cases, may be misleading.

The UMN data not only covered a useful range for the Reynolds numbers and FSTI values, but also provided detailed measurements of pressure distribution, boundary-layer velocity, turbulence intensity, and intermittency profiles on the suction surface (from P2 to P13 stations, $0.045 < s/L_{ss} < 0.93$). It offers a good test case to validate the current approach in predicting the physics involved in the complex interplay between flow separation and transition.

III. Transport Model for the Intermittency

In this section, the transport model for intermittency is presented. More detailed description of the development and implementation of the model is given by Suzen and Huang.[12,13]

The main objective in the development of the transport model is to be able to predict flow transition under the effects of freestream turbulence and Reynolds number variations. To accomplish this objective, the model must accurately produce the intermittency distribution under diverse operating flow conditions. Furthermore, the model should reproduce the intermittency distribution of Dhawan and Narasimha[7] in the streamwise direction and at the same time give rise to a realistic variation of intermittency in the cross-stream direction. The intermittency transport equation of Steelant and Dick[5] posseses one of these desired properties: It is formulated such that the model reproduces the γ distribution of Dhawan and Narasimha[7] in the streamwise direction. However, the model does not take the variation of γ in the cross-stream direction into consideration. On the other hand, the γ equation of the k–ϵ–γ turbulence model of Cho and Chung[14] provides a realistic profile of γ in the cross-stream direction, and this model has been previously adopted by Savill[15] and used in combination with a low-Reynolds-number Reynolds stress transport model in the computation of bypass transition flows.

The current intermittency transport model blends the transport equation models of Steelant and Dick[5] and Cho and Chung[14] into one transport equation to combine the desired properties of each model, namely, the ability to produce the streamwise γ distribution of Dhawan and Narasimha[7] and to provide a realistic variation of intermittency in the cross-stream direction.

The blending is achieved by formulating the generation term of the model as a combination of the generation terms of Steelant and Dick's[5] model and Cho and Chung's[14] model. The transport equation for intermittency has the following form:

$$\frac{\partial \rho\gamma}{\partial t} + \frac{\partial \rho u_j \gamma}{\partial x_j} = (1-\gamma)[(1-F)T_0 + F(T_1 - T_2)] + T_3 + D_\gamma \quad (2)$$

The first term, T_0, is from Steelant and Dick.[5] It aims to reproduce the intermittency distribution of Dhawan and Narasimha.[7] The formulation for T_0 is given by

$$T_0 = 2C_0\rho\sqrt{u_k u_k}\, f(s) f'(s) \quad (3)$$

where ρ is the fluid density, u_k is the velocity component, and the distributed breakdown function $f(s)$ has the form

$$f(s) = \frac{as'^4 + bs'^3 + cs'^2 + ds' + e}{gs'^3 + h} \quad (4)$$

where $s' = s - s_t$, s is the distance along the streamline coordinate and s_t is the transition location. The coefficients are

$$a = 50\sqrt{n\sigma/U}, \qquad b = -0.4906, \qquad c = 0.204(n\sigma/U)^{-0.5}$$
$$d = 0.0, \qquad e = 0.04444(n\sigma/U)^{-1.5}$$
$$h = 10e, \qquad g = 50 \quad (5)$$

Two major production terms from Cho and Chung's[14] model are T_1 and T_2. These two terms are used in the form $(T_1 - T_2)$ in the model. The term T_1 mimics the production of turbulence kinetic energy P_k and is given by

$$T_1 = C_1\gamma\frac{P_k}{k} = \frac{C_1\gamma}{k}\tau_{ij}\frac{\partial u_i}{\partial x_j} \quad (6)$$

with the shear stresses defined as

$$\tau_{ij} = \mu_t\left[\frac{\partial u_i}{\partial x_j} + \frac{\partial u_j}{\partial x_i} - \frac{2}{3}\frac{\partial u_k}{\partial x_k}\delta_{ij}\right] - \frac{2}{3}\rho k\delta_{ij} \quad (7)$$

The term T_2 represents the production resulting from the interaction between the mean velocity and the intermittency field and is given by

$$T_2 = C_2\gamma\rho\frac{k^{\frac{3}{2}}}{\epsilon}\frac{u_i}{(u_k u_k)^{\frac{1}{2}}}\frac{\partial u_i}{\partial x_j}\frac{\partial \gamma}{\partial x_j} \quad (8)$$

The production terms T_0 and $(T_1 - T_2)$ are blended by using a function F to facilitate a gradual switching from T_0 to $(T_1 - T_2)$ inside the transition region:

$$P_\gamma = (1-F)T_0 + F(T_1 - T_2) \quad (9)$$

A nondimensional parameter, $k/W\nu$, is chosen to construct the blending function F, where k is the turbulence kinetic energy and W is the magnitude of the vorticity. This parameter increases rapidly with distance away from the wall inside the transition region. To achieve a gradual switching from T_0 to $(T_1 - T_2)$, the following blending function is proposed:

$$F = \tanh^4\left[\frac{k/W\nu}{200(1-\gamma^{0.1})^{0.3}}\right] \quad (10)$$

As can be seen from Eq. (10), when $k/W\nu \gg 200(1-\gamma^{0.1})^{0.3}$, $F = 1$, and the model switches to Cho and Chung's[14] model; when $k/W\nu \ll 200(1-\gamma^{0.1})^{0.3}$, $F = 0$, and the model becomes Steelant and Dick's[5] model. Outside the transition zone, the model switches to Cho and Chung's[14] model, except for the very thin region close to the wall.

An additional diffusion-related production term is introduced by Cho and Chung[14] as

$$T_3 = C_3\rho\frac{k^2}{\epsilon}\frac{\partial \gamma}{\partial x_j}\frac{\partial \gamma}{\partial x_j} \quad (11)$$

This term is kept active over the entire flowfield, and no blending is applied to this term.

Diffusion of γ is represented by the following term:

$$D_\gamma = \frac{\partial}{\partial x_j}\left\{[(1-\gamma)\gamma\sigma_{\gamma_l}\mu + (1-\gamma)\sigma_{\gamma_t}\mu_t]\frac{\partial \gamma}{\partial x_j}\right\} \quad (12)$$

The final transport equation for intermittency takes the following form:

$$\frac{\partial \rho\gamma}{\partial t}+\frac{\partial \rho u_j\gamma}{\partial x_j}=(1-\gamma)\Bigg[(1-F)2C_0\rho\sqrt{u_k u_k}f(s)f'(s)$$
$$+F\left(\frac{C_1\gamma}{k}\tau_{ij}\frac{\partial u_i}{\partial x_j}-C_2\gamma\rho\frac{k^{\frac{3}{2}}}{\epsilon}\frac{u_i}{(u_k u_k)^{\frac{1}{2}}}\frac{\partial u_i}{\partial x_j}\frac{\partial \gamma}{\partial x_j}\right)\Bigg]$$
$$+C_3\rho\frac{k^2}{\epsilon}\frac{\partial \gamma}{\partial x_j}\frac{\partial \gamma}{\partial x_j}+\frac{\partial}{\partial x_j}\Bigg\{\Big[(1-\gamma)\gamma\sigma_{\gamma_l}\mu$$
$$+(1-\gamma)\sigma_{\gamma_t}\mu_t\Big]\frac{\partial \gamma}{\partial x_j}\Bigg\} \tag{13}$$

where,

$$\sigma_{\gamma_l}=\sigma_{\gamma_t}=1.0, \qquad C_0=1.0, \qquad C_1=1.6$$
$$C_2=0.16, \qquad C_3=0.15$$

The intermittency is incorporated into the computations by the use of the eddy viscosity μ_t^*, which is obtained by multiplying the eddy viscosity obtainable from a turbulence model μ_t with the intermittency factor γ. That is, $\mu_t^*(=\gamma\mu_t)$ is used in the diffusive parts of the mean flow equations.

To allow the intermittency to have full control of the transitional behavior, the turbulence model selected to obtain μ_t must produce fully turbulent features before the flow transition takes place. The SST model of Menter[11] is found to satisfy this requirement. It produces fully turbulent flow behavior immediately after the leading edge of the boundary layer, and, therefore, it is used as a baseline model to compute μ_t and other turbulence quantities in the calculations.

The value of $n\sigma$ used in evaluating the constants given by Eq. (5) is provided by the Mayle[16] correlation for zero-pressure gradient flows:

$$\hat{n}\sigma=1.8\times10^{-11}Tu^{\frac{7}{4}} \tag{14}$$

The value of $n\sigma$ is obtained with the definition $\hat{n}=n\nu^2/U^3$. Note that a value of 1.8×10^{-11} was used in the current work to give a slightly better fit of the data of Gostelow et al.[17] When flows are subject to pressure gradients, the following correlation is used:

$$\frac{\hat{n}\sigma}{(\hat{n}\sigma)_{\mathrm{ZPG}}}=\begin{cases}M^{[1-\exp(0.75\times10^6 K_t Tu^{-0.7})]}, & K_t<0\\ 10^{-3227K_t^{0.5985}}, & K_t>0\end{cases} \tag{15}$$

with M defined as

$$M=(850Tu^{-3}-100Tu^{-0.5}+120)$$

where $(\hat{n}\sigma)_{\mathrm{ZPG}}$ is the value for zero pressure gradient obtained from Eq. (14) and $K_t=(\nu/U_t^2)(\mathrm{d}U/\mathrm{d}x)_t$ is the flow acceleration parameter. The favorable pressure gradient part of the preceding correlation (for $K_t>0$) is from Steelant and Dick.[5] The portion of the correlation for adverse pressure gradient flows, $K_t<0$, is formulated using the transition data of Gostelow et al.[17] and Simon et al.[10] The data and the correlation are shown in Fig. 3. The Gostelow et al. data are for attached flat-plate boundary layers, and they are in a relatively mild adverse pressure gradient range when compared to the Simon et al. low-pressure turbine experiments, where flow separation and transition mostly occur. Note from Fig. 3 that Eq. (15) captures the trend of two groups of data very well. The data show some scattering in Fig. 3 for small K_t with high Tu values, whereas the correlation is forced to take a value of unity. The current study uses the intermittency transport model to obtain the intermittency distribution for the transitional flows, with the onset of transition defined according to the following two flow possibilities.

A. Separated-Flow Transition

Roberts[18] proposed a semi-empirical theory to predict onset of transition within a laminar separation bubble over the airfoil suction surface. The transition Reynolds number Re_{st}, which is based on the length defined between the onset location of separation and that of transition, is correlated as a function of a turbulent factor representing effects of the external turbulence level and its disturbance spectrum. The model was simplified by Davis et al.[19] to only a function of turbulence intensity:

$$Re_{\mathrm{st}}=2.5\times10^4\log_{10}\coth(0.1732Tu) \tag{16}$$

where Tu is the FSTI value at the onset of separation. Although this model was originally proposed for swept wing flows, Simon et al.[10] observed that the correlation matches their experiments well. The present paper, therefore, adopts the Davis et al.[19] correlation to predict the onset of separated-flow transition.

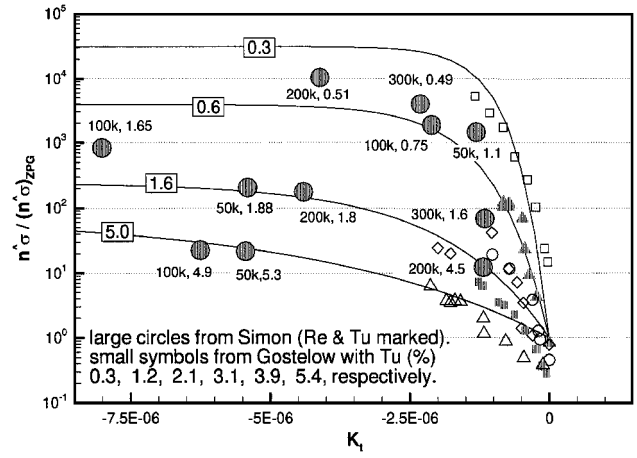

Fig. 3 New transition length correlation.

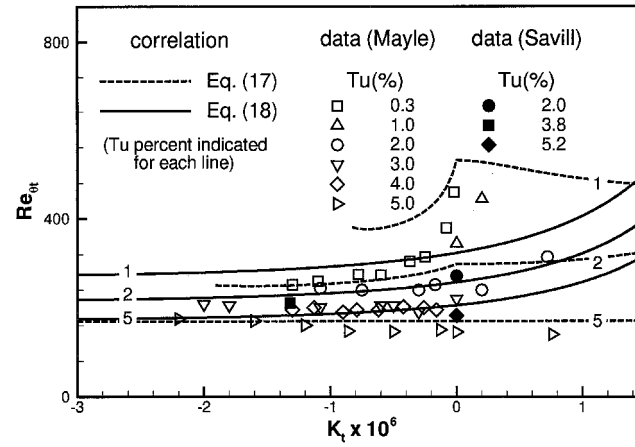

Fig. 4 Correlation for attached-flow transition.

B. Attached-Flow Transition

Abu-Ghannam and Shaw[20] suggested that the onset of transition for attached flows can be obtained by correlating the boundary-layer momentum thickness Reynolds number to the FSTI according to

$$Re_{\theta t}=163+\exp\{F(\lambda_\theta)-[F(\lambda_\theta)/6.91]Tu\} \tag{17}$$

where

$$F(\lambda_\theta)=6.91+12.75\lambda_\theta+63.64\lambda_\theta^2 \qquad \text{for} \qquad \lambda_\theta<0$$
$$F(\lambda_\theta)=6.91+2.48\lambda_\theta-12.27\lambda_\theta^2 \qquad \text{for} \qquad \lambda_\theta>0$$

Although the Abu-Ghannam and Shaw[20] correlation showed good agreement with experimental data for flows with zero and adverse pressure gradients, the model is not very sensitive to flows with strong favorable pressure gradients, as shown in Fig. 4, in which one would expect the transition to be delayed as a result of flow acceleration.

To allow for a more sensitive response to strong favorable pressure gradients while maintaining the good features of the Abu-Ghannam and Shaw[20] correlation in an adverse pressure gradient region, the transition criterion was recorrelated to the FSTI Tu and the acceleration parameter K_t according to

$$Re_{\theta t} = \left(120 + 150 Tu^{-\frac{2}{3}}\right) \coth\left[4\left(0.3 - K_t \times 10^5\right)\right] \qquad (18)$$

where K_t was chosen as the maximum absolute value of the acceleration parameter in the downstream deceleration region. Equation (18) was designed to have a better fit of the available experimental data. As can be seen from Fig. 4, except for data with very low FSTI values (less than 1%), Eq. (18) seems to correlate well with the existing experimental data. For transition under very low turbulence intensity, the current correlation exhibits more characteristics of natural transition behavior than bypass transition. Finally, although the correlation fits the transition data well for flows under adverse pressure gradients, it was purposely designed to rise rapidly as K_t becomes positive (favorable pressure gradients). This measure is taken to reflect that the flow transition may be delayed when subject to favorable pressure gradients.

Detailed comparisons of the current intermittency transport model with the T3 benchmark test cases of Savill[1,2] were conducted by Suzen and Huang.[13] To illustrate the effectiveness of the intermittency concept over the pure turbulence models (namely, the k–ϵ model of Launder and Sharma,[21] the k–ω model of Wilcox,[22] and the SST of Menter[11]) in predicting flow transition, the T3C2 experiment of Savill[1,2] is repeated here as a test case. The T3C2 case is one of the test cases specially designed to test the ability of turbulence models in predicting transition with continuous variation in pressure gradient, representing an aft-loaded turbine blade.

The computations for this case were performed with a boundary-layer code that solves the mean flow, turbulence model, and intermittency equations using a second-order finite volume method. In the computations, 175 grid points, expanding from the wall to the freestream, were used in the cross-stream direction. The y^+ values for the first grid point away from the wall were between 0.1 and 0.15. The solutions were obtained by using 1000 streamwise steps. This corresponds to a maximum nondimensional step size of $\Delta x^+ = 37$.

The T3C2 case has an inlet Reynolds number of 3.5×10^5 per meter and a freestream turbulence intensity of 2.8% at the leading edge. The inlet conditions for the turbulence length scale were calibrated to match the experimental freestream turbulence decay. For example, in the present study, the turbulence kinetic energy was fixed according to the experimental freestream turbulence level and the matching of the freestream turbulence decay provided the estimated value of the dissipation rate of turbulence kinetic energy ϵ (or the value of μ_t/μ) at the inlet. After matching the decay of freestream turbulence, it was determined that a value of $\mu_t/\mu = 5$ was needed for the SST model[11] and the Launder–Sharma[21] k–ϵ model, and 5.6 was used for Wilcox's[22] k–ω model at the inlet. The onset of transition was specified at $Re_{\theta_t} = 297$, according to Eq. (18).

The predicted skin-friction coefficient distributions were compared with experimental data in Fig. 5. As can be seen from the comparison, Menter's[11] SST model and Wilcox's[22] k–ω model gave immediate transition to turbulence at the leading edge, showing almost no laminar zone. The k–ϵ model of Launder–Sharma[21] predicted a too early transition, and the length of transition to turbulence is somewhat too short when compared to experimental data. In contrast, the current transition model predicted the length of the transition region well and showed very good comparison with the data.

One of the major features of the current model is its ability to reproduce realistic cross-stream intermittency profiles. The predicted intermittency profiles at various streamwise stations through the transition zone are shown in Fig. 6. The profiles exhibit a peak between $y/\delta^* = 1$ and 2, then drop off toward zero near the edge of the boundary layer, around $y/\delta^* = 8$. These features are consistent with the trends observed in experimental data of Sohn and Reshotko[23] and Gostelow and Walker.[24]

The results obtained for the T3C2 case clearly showed the superior predicting capabilities of the current model and the effectiveness

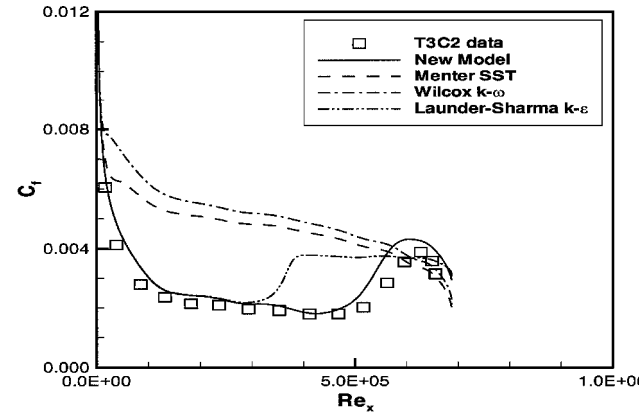

Fig. 5 Comparison of the skin-friction coefficient for variable pressure gradient flow (T3C2 case).

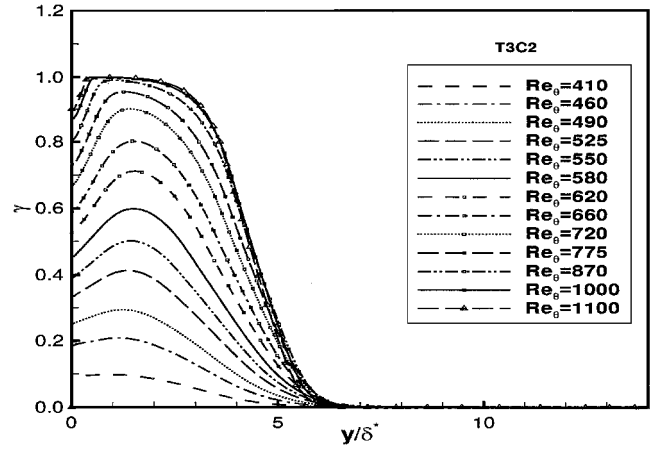

Fig. 6 Cross-stream intermittency profiles for variable pressure gradient flow (T3C2 case).

of the intermittency concept over the pure turbulence models for predicting transitional flows.

To demonstrate the ability of the current intermittency model in predicting general turbine configurations, the experiment of Simon et al.[10] was selected as a test case. In the prediction of more general turbine flows in which transition can take place either in an attached- or a separated-flow situation, the present study used a prediction–correction scheme to compute flow transition. First, for a given Reynolds number, numerical calculation is carried out under the assumption that the entire flow is laminar. The resultant onset position of separation is determined from the laminar solution and defined as the laminar separation point. In the current study, this location was not very sensitive to the Reynolds number range considered because separation was mainly determined by the geometry of the blade. Second, by applying the Davis et al.[19] correlation, Eq. (16), to the laminar solution, the onset point of transition was determined. Whereas the computation was started using the laminar solution, the onset point of transition was updated at each 100 iterations by reapplying the Davis et al.[19] correlation to the most recent solution.

As the transition point moves upstream, there is a tendency for the separation point to move downstream. If the process converges to a solution in which the length between the onset of separation and the onset of transition satisfies Eq. (16), the final solution is established and a flow with separated-flow transition is assumed. On the other hand, as the newly predicted separation point moves downstream of the prescribed transition point, or as the separation bubble disappears, the calculation is performed with the correlation for the onset of transition [Eq. (16)] being replaced by the attached-flow correlation [Eq. (18)]. The final solution may or may not contain flow separation. If a flow separation indeed occurs, the onset of transition may well be in the attached flow region, and, therefore, the

use of Eq. (18) is justified. This updating scheme usually converges after around 10 updates.

IV. Numerical Aspects

All computational results presented herein were obtained by the TURCOM code developed by Huang and Coakley.[9] TURCOM contains a variety of turbulence models, ranging from one-equation to Reynolds stress transport equation models, and was designed to validate the performance of turbulence models. This code has been validated against a wide range of flow configurations and conditions, including several hypersonic, transonic, and subsonic flows.[9,25–27]

In the present work, we have made a special attempt to mimic the exact experimental conditions (see Fig. 1). The calculations were performed in a channel with the inlet boundary provided at one chord length upstream of the turbine blade. A cubic spline fit of the surface of the turbine blade was used to set up the pressure and suction walls in the channel. A flat plate was attached to the trailing edge of the suction surface to simulate the extended flow-guiding wall used in the experiment. The computational domain downstream of the pressure wall was allowed to expand at an angle of 15 deg in an attempt to capture the shear flow development. The total pressure and the total temperature were prescribed at the inlet according to the experiment. A slip boundary condition was applied to the channel surfaces ahead of the blade surfaces. The two blade surfaces, as well as the downstream extension wall, were assumed to be adiabatic with the no-slip condition. A constant pressure boundary condition was applied to the exit plane and the outer entrainment boundary downstream of the pressure surface.

All calculations were made using the H grid. The grid sensitivity study was first performed in a linear cascade situation by employing inviscid calculation for the same turbine blade used in the UMN study. The predicted pressure coefficients were compared with the design curve provided by the blade manufacturer, and the study offers us a useful guide to the choice of optimal computational grid distribution. Figure 7a shows the comparison of pressure coefficient profiles along the airfoil suction surface using 400×200 and 300×150 grids, in which the grids were uniform in the streamwise direction and expanded in the cross-stream direction with the first wall unit grid spacing y^+ approximately equal to 0.5. It can be seen that the pressure coefficient distributions given by the two grids are essentially the same. On the other hand, when the 200×100 and 100×50 grids are used, the pressure distributions are slightly lower

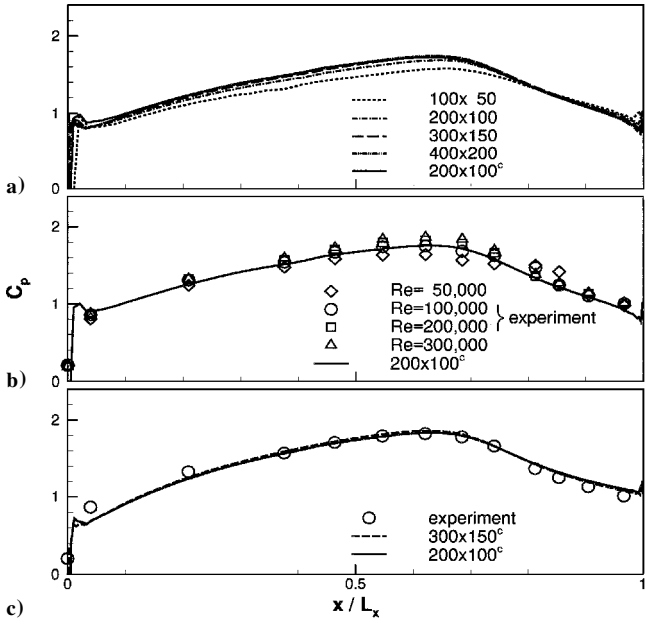

Fig. 7 Grid sensitivity study comparison of the surface pressure coefficient distributions: a) inviscid cascade, b) inviscid cascade, and c) viscous calculation of the experiment of Simon et al.,[10] $Re = 2 \times 10^5$ and FSTI = 10%.

than the fine-grid solutions. If the grid distribution along the streamwise direction were clustered in both the leading-edge and trailing-edge regimes, the same pressure coefficients as obtained by the 400×200 grid could be achieved by a 200×100 grid. The solution is marked by a superscript c, that is, (200×100^c), in Fig. 7a. This result is compared with the experiment data, as shown in Fig. 7b. Note that the pressure coefficients obtained here are essentially the same as those of the design curve given by the blade manufacturer and UMN data. Using the same numerical grid clustering as used in 200×100^c, we performed a viscous calculation of the experiment setup (noncascade) for the flow with $Re = 2 \times 10^5$ and FSTI = 10%. Two sets of grids, 300×150^c and 200×100^c, were used to perform the calculation. Note that both grids are clustered grids and are indicated in Fig. 7c with a superscript c. Note from Fig. 7c that the solutions obtained from these two grids were almost the same, and they both agree with the experiment fairly well. All numerical results reported hereafter were based on the 200×100^c grid.

One of the important details in UMN data is the bleeding of the flow upstream of the airfoil surfaces (see Fig. 1). The purpose of the bleeds is to eliminate the incoming boundary layers. However, it was found that the bleed at the leading edge of the suction wall has a large effect on the solution in the upstream region of the suction surface. The leading-edge bleed was simulated in the numerical calculations by the application of a uniform suction to a small gap just upstream of the leading edge of the suction wall. The magnitude of the suction was adjusted to match the experimental velocity profiles in the first few stations. Numerical tests were carried out under three different Reynolds numbers with and without the leading-edge bleed, and the results are shown in Fig. 8 together with UMN data. As can be seen from Fig. 8, without the leading-edge bleed the solutions exhibit a (laminar) boundary layer that is much too thick in the beginning portion of the airfoil surface. On the other hand, the results obtained with the leading-edge bleed can be made to match the velocity profiles from P2 to P7 stations very well for all three Reynolds numbers, as shown in Fig. 8. This adjustment of the flow is crucial because the downstream development of the flow is strongly dependent on the events taking place in the upstream region of the blade.

Figure 9 shows the comparison of results obtained by the current transition model with two other pure turbulence model predictions, one with the Launder–Sharma[21] k–ϵ model and the other with the SST model.[11] The UMN experimental flow with $Re = 1 \times 10^5$ and FSTI = 10% has been chosen for comparison. Predictions of velocity profiles for all measured stations, P2–P13, are given in Fig. 9. Not surprisingly, the main drawback of the SST model is that it predicted a too early transition to turbulence. Because the model predicted a too early flow transition to turbulence, the SST model predicted no flow separation. On the other hand, although the k–ϵ model predicted the upstream development of the flow very well, the velocity profiles in the downstream portion were poorly represented. Overall, the current transition model showed the best performance throughout the airfoil suction surface.

Finally, because the current approach uses an integral parameter of the boundary layer, θ, to predict attached flow transition, the ability of the model in predicting momentum thickness becomes important and needs verification. Figure 10 shows the comparison of the momentum thickness along the suction surface for three representative cases: $Re = 2 \times 10^5$ and FSTI = 2.5%, $Re = 2 \times 10^5$ and FSTI = 10%, and $Re = 3 \times 10^5$ and FSTI = 2.5%. As can be seen from Fig. 10, the agreement between predictions and measurements is excellent, especially in the upstream laminar flow region.

V. Results and Discussion

The current transition model was applied to predict the UMN experiment under a range of flow conditions, covering four Reynolds numbers and two FSTI values. The objectives of this study are twofold. First, the approach is validated against the experiment to address the issue of Reynolds number and freestream turbulence effects. Second, the parametric study of Reynolds number and freestream turbulence effects serves to provide useful physical insights into the complex interplay between transition and separation over the airfoil suction surface.

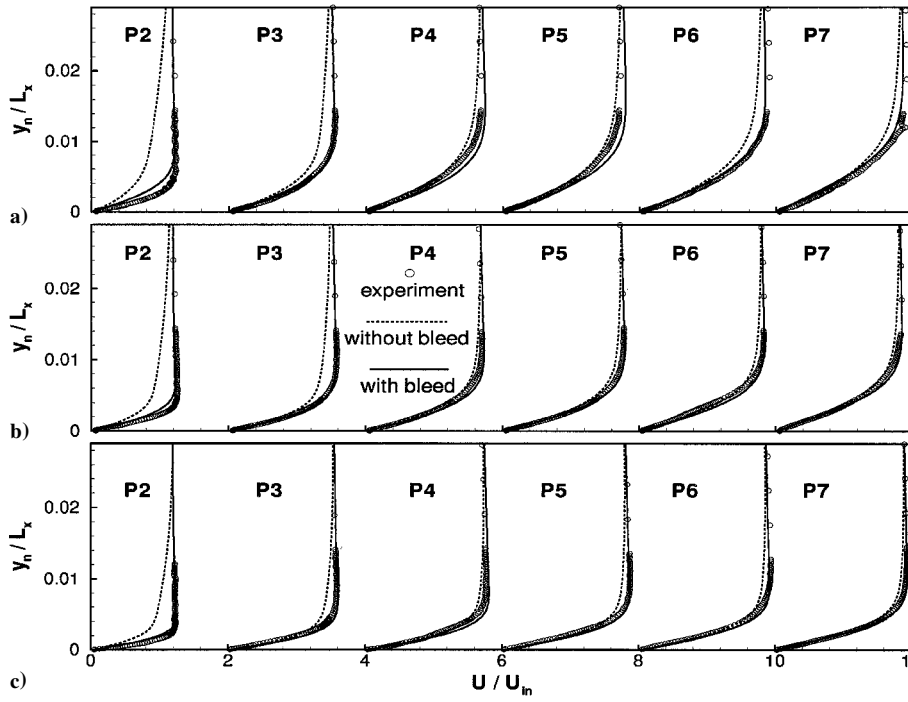

Fig. 8 Boundary treatment of the leading-edge bleed: a) $Re = 5 \times 10^4$ and FSTI = 10%, b) $Re = 1 \times 10^5$ and FSTI = 10%, and c) $Re = 2 \times 10^5$ and FSTI = 10%.

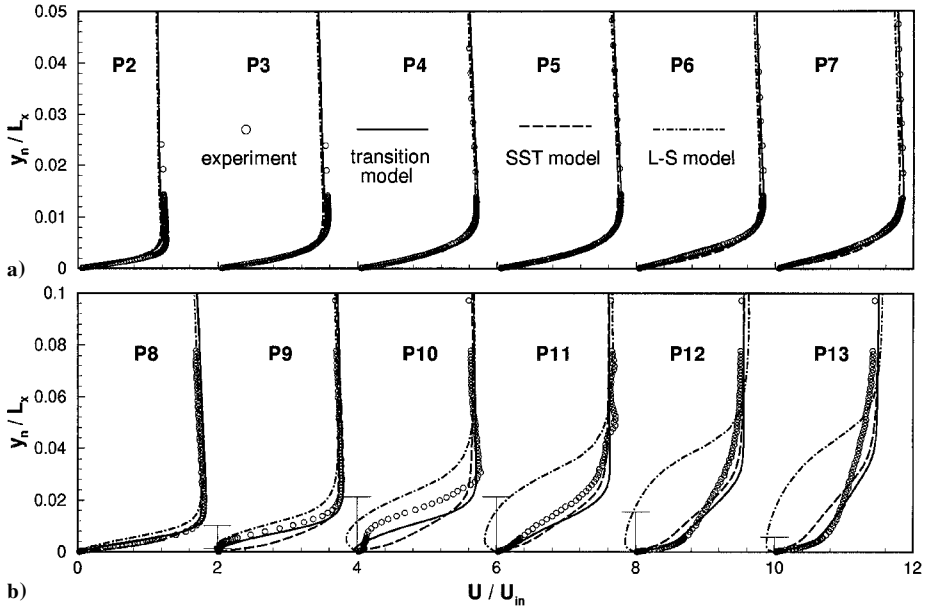

Fig. 9 Comparison of velocity profiles, transition model vs pure turbulence models: a) P2–P7 stations and b) P8–P13 stations.

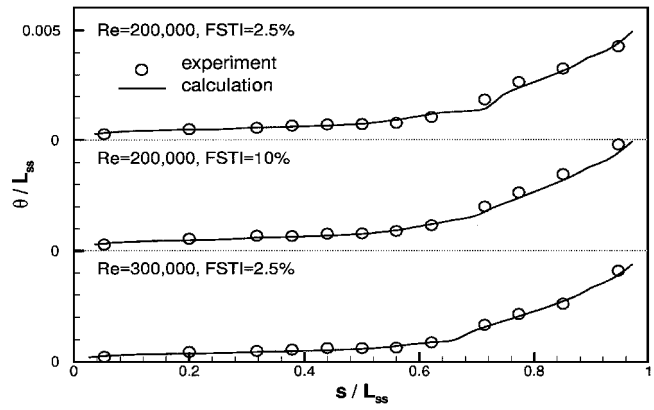

Fig. 10 Comparison of boundary-layer momentum thickness.

Two FSTI values were considered: one with FSTI = 10% and the other with FSTI = 2.5%. For the cases with FSTI = 10%, three Reynolds numbers were chosen, $Re = 5 \times 10^4$, 1×10^5, and 2×10^5. For the FSTI = 2.5% cases, Reynolds numbers selected were $Re = 1 \times 10^5$, 2×10^5, and 3×10^5. These cases were selected to test the model's ability to capture the desired behavior of flow pattern variations caused by the changes in flow conditions. Figure 11 shows velocity vectors and streamlines against changes of FSTI and Reynolds number predicted by the intermittency approach. Note that these plots were magnified by a factor of eight in the cross-stream direction. The predicted onset position of transition for each flow was denoted by t in the insets of Fig. 11. For the low-Reynolds-number case ($Re = 5 \times 10^4$ and FSTI = 10%), the flow exhibits a remarkable separation region that begins in a location between the P8 and P9 stations and extends to the P12 station (Fig. 11a), and transition occurs between the P9 and P10 positions in the separation bubble. When FSTI is kept the same while the Reynolds number is increased

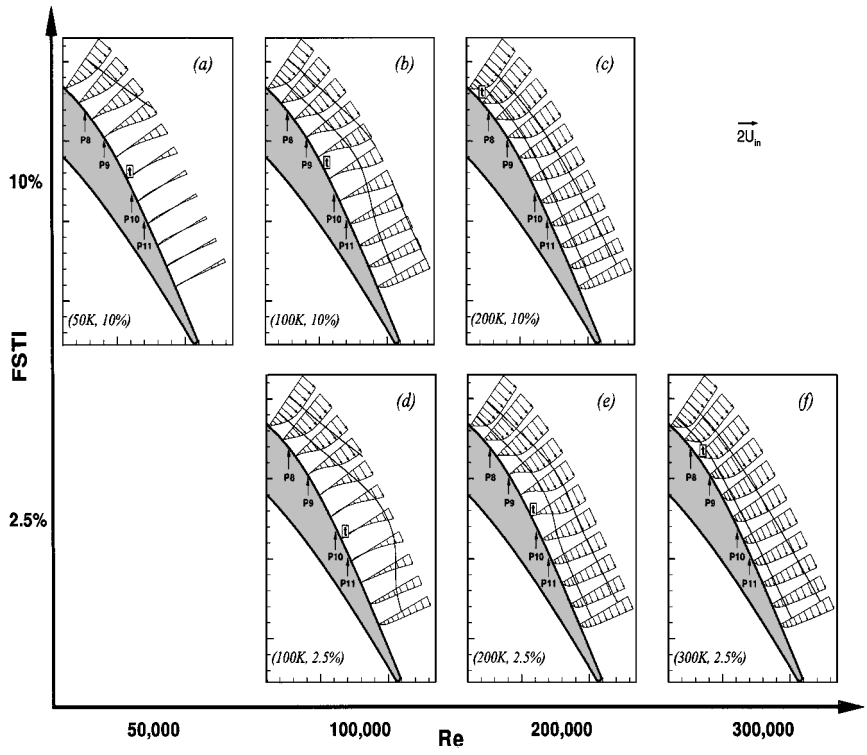

Fig. 11 Overall view of a low-pressure turbine flow subject to effects of Reynolds number and freestream turbulence intensity.

to $Re = 1 \times 10^5$, it is observed that the transition onset moves upstream (still between the P9 and P10 positions), and the separation bubble is suppressed (Fig. 11b). If the Reynolds number is increased to $Re = 2 \times 10^5$ while the same FSTI is kept, the prediction shows that the transition onset moves even farther upstream (before the P8 position), and the separation bubble disappears, whereas the experiment shows a tiny and thin separation (Fig. 11c). On the other hand, if the Reynolds number is kept at $Re = 2 \times 10^5$ while FSTI is dropped from 10 to 2.5%, the transition onset moves downstream close to the P10 position, and the separation bubble reappears (Fig. 11e). If the same value of FSTI is kept while the Reynolds number is increased from $Re = 2 \times 10^5$ to 3×10^5, the transition onset moves upstream again to approximately the P8 position, and the separation bubble again disappears (Fig. 11f). On the other hand, if Reynolds number is decreased from $Re = 2 \times 10^5$ to 1×10^5, the transition onset point moves downstream to a location between stations P10 and P11, and the separation bubble becomes larger (Fig. 11d).

Detailed comparisons of the pressure and velocity profiles between the computation and the experiment are provided as follows: Figures 12a, 13a, 14a, 15a, and 16a correspond to pressure coefficient distribution along the suction surface; Figs. 12b, 13b, 14b, 15b, and 16b are variations of the freestream velocity; Figs. 12c, 13c, 14c, 15c, and 16c are velocity profiles for P2 to P7 stations; and Figs. 12d, 13d, 14d, 15d, and 16d are velocity profiles for P8 to P13 stations.

The flow with $Re = 5 \times 10^4$ and FSTI = 10% displays a large separation bubble, although its FSTI is high. The experiment showed that the flow did not turn fully turbulent by the end of the suction wall. In the calculation, the onset of transition predicted by Eq. (16) was located between the P9 and P10 stations. The calculations seem to agree with the experimental observations. As can be seen from Fig. 12a, the measurement exhibited a pressure plateau in the separation region (between P9 and P11) and a sudden drop of the surface pressure coefficient at the P12 station due to flow reattachment. These features were well captured by the calculation.

The (laminar) velocity profiles of the boundary layer in the upstream portion of the suction surface compared fairly well with the data, with the exception that some small differences were observed in the P2, P4, and P5 stations, shown in Fig. 12c. The small discrepancy in the P2 station may be because the boundary condition treatment of the leading-edge bleed is more sensitive to the solution for the flow at this low Reynolds number. The differences between the calculation and the experiment observed in the P4 and P5 stations may be caused by the uncertainties of measurements because they are accompanied by an unusual small drop of the experimental freestream velocity, as shown in Fig. 12b.

The comparison of the velocity profiles over P8–P13 stations shows a good prediction of the separation bubble (Fig. 12d). The present computation reconfirms that the flow separates between the P8 and P9 stations, reattaches after the P12 station, and returns a correct size of the separation bubble. The strange experimental behavior (all positive values) in the near-wall region at the P11 and P12 stations was due to the inability of the single hot-wire probe to resolve reverse flow.[10] The predicted profiles at the P12 and P13 stations do not agree very well with the experiment. We considered that these errors may be caused by the following two factors. First, the experiments suggested that the turbulence intensity in these regions may be very high, and, therefore, the errors may be caused by the experimental measurements. To clarify this issue, we have shown a number of vertical error bars in Figs. 10–14 to indicate regions of high local turbulence intensity (regions with turbulence intensity larger than 30%). Second, the current turbulence model is incapable of predicting flow recovery after reattachment. (Huang[25] reported that none of the popular one- and two-equation models, including the SST model, can correctly predict flow recovery after flow reattachment.)

When the Reynolds number Re was increased to 1×10^5 while FSTI was kept at 10%, the velocity adjacent to the suction surface of the blade increased due to the increasing momentum transport in the near-wall region. As a result, a smaller separation bubble was observed as compared to the flow with $Re = 5 \times 10^4$. As can be seen from Fig. 13a, the measured pressure coefficient distribution gave a shorter plateau in the region from the P9 to P10 stations, followed by a sudden drop of pressure coefficient in the P11 station. Again, these features were well captured by the current calculation. Figure 13b shows that the predicted variation of the freestream velocity is in very good agreement with the experiment. Note from Fig. 13c that the (laminar) velocity profiles in the upstream portion of the suction surface agree very well with the experiment. The onset of transition predicted by the Davis et al.[19] correlation [Eq. (16)] moved slightly farther upstream than that in the earlier case. As a combined result of an increased Reynolds number and an earlier transition, the size

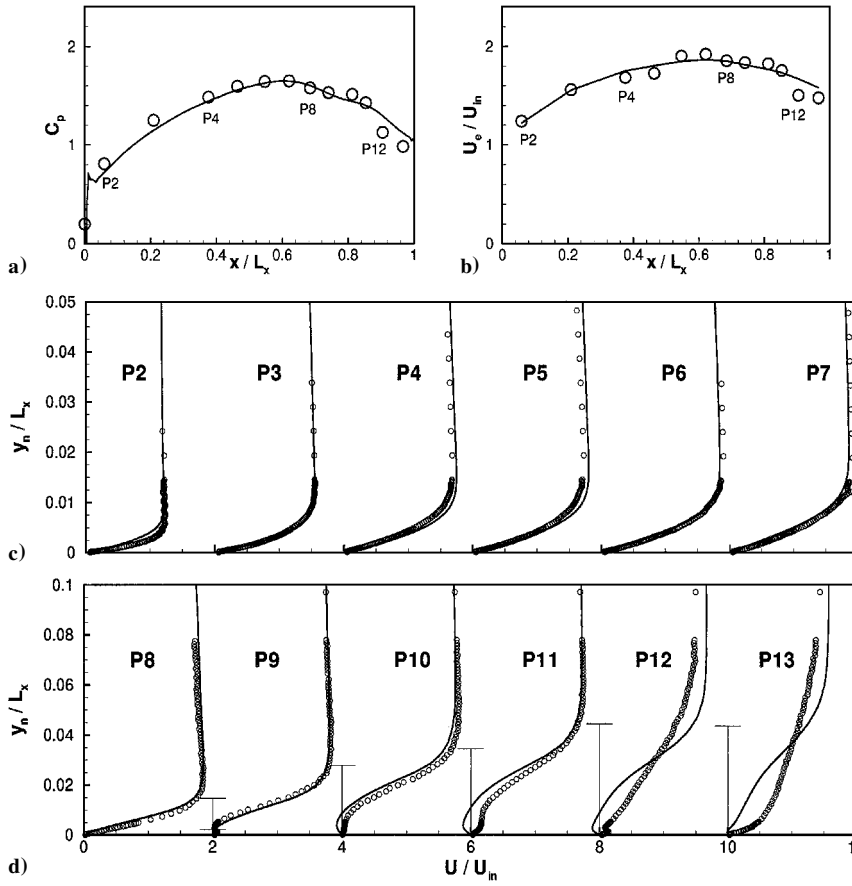

Fig. 12 Prediction of the low-pressure turbine experiment: $Re = 5 \times 10^4$ and FSTI = 10%.

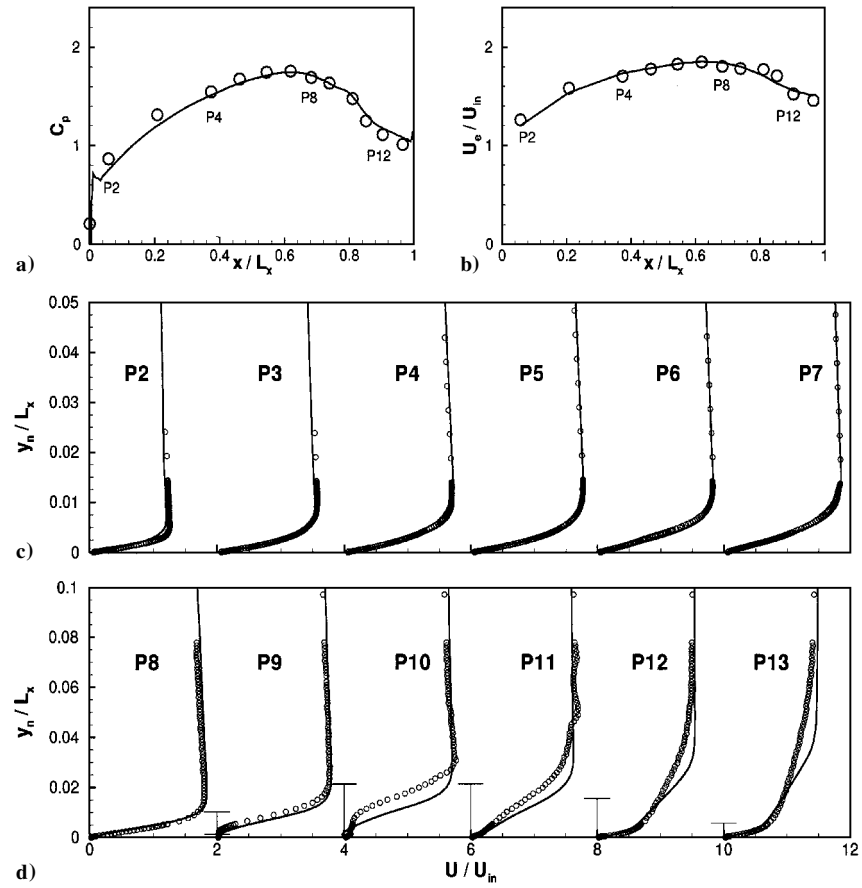

Fig. 13 Prediction of the low-pressure turbine experiment: $Re = 1 \times 10^5$ and FSTI = 10%.

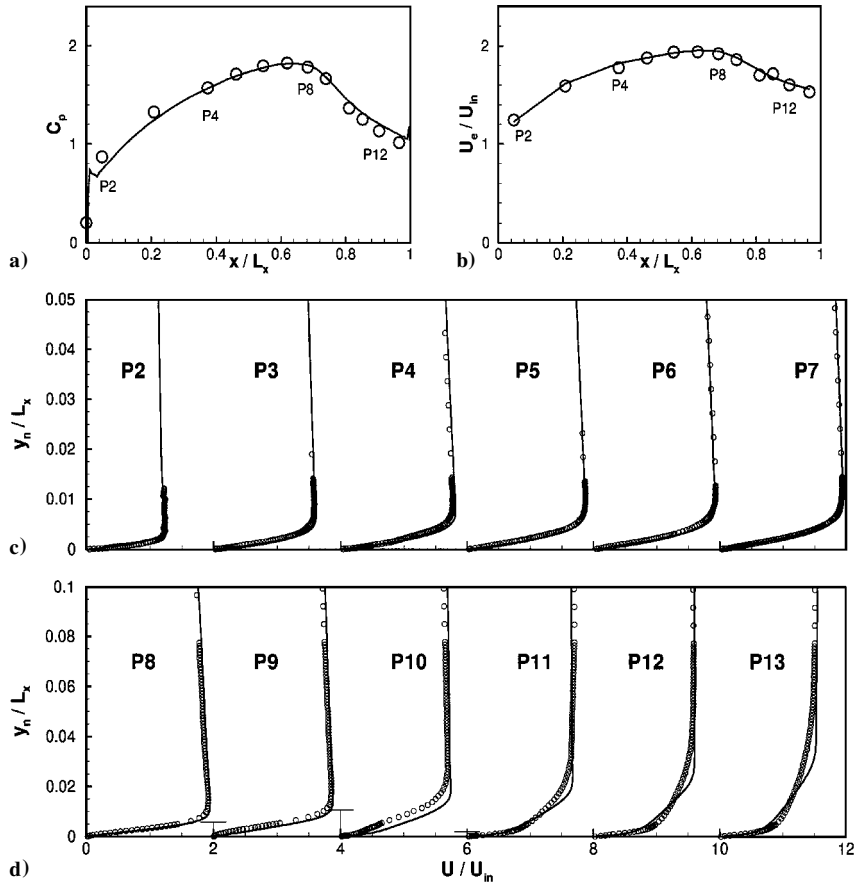

Fig. 14 Prediction of the low-pressure turbine experiment: $Re = 2 \times 10^5$ and FSTI = 10%.

of the separation bubble is reduced. Figure 13d shows that the flow reattached at the P11 station, agreeing very well with the experimental observation. The predicted velocity profiles at the P12 and P13 stations agreed better with the experiment than they did in the flow with $Re = 5 \times 10^4$.

As the Reynolds number was further increased to $Re = 2 \times 10^5$, while FSTI was kept at 10%, the calculation showed that the separation bubble disappeared. Note that, to predict this case, we first used Eq. (16) to locate the onset of transition by starting from the laminar solution. As the solution advanced, the separation bubble disappeared (even though the experiment suggested a small separation zone), and we switched to Eq. (18) to predict the onset of transition. In this case, the onset of transition was located just before the P8 station, which is the farthest upstream position for all of the cases we have considered. As can be seen from the comparison of the pressure coefficient distribution shown in Fig. 14a, there is no apparent pressure plateau. Figure 14b shows that the predicted variation of the freestream velocity is in excellent agreement with the data. The velocity profiles on the suction surface are predicted reasonably well, as can be seen from Figs. 14c and 14d. The experiment did suggest, however, that a very tiny separation zone was observed between the P9 and P10 stations. Because the separation bubble was very tiny, the measured velocity profiles in both the P9 and P10 stations did not show signs of reversed flow (Fig. 14d).

Next, the Reynolds number was maintained at $Re = 2 \times 10^5$ while FSTI was reduced to 2.5%. The measurement and the prediction both showed that this flow had a separation zone starting before the P9 and ending downstream of the P10 stations. Comparisons of the pressure coefficient distribution and the variation of the freestream velocity showed good agreement between the prediction and the measurement (Figs. 15a and 15b, respectively). Figure 15c shows that the agreement of the (laminar) velocity profiles in the upstream portion of the suction surface is excellent. The agreement of the velocity profiles in the downstream portion of the suction surface is also reasonable (Fig. 15d). The reason for the defect of the experimental data as appeared in the near wall region of the P10 station is attributed to the inability of the hot wire to measure reversed flows, as mentioned before.

The next case holds FSTI = 2.5% while the Reynolds number is increased to $Re = 3 \times 10^5$. Because the calculation showed no flow reversal (whereas the experiment suggested a very small separated flow region), the computation was performed following the same procedure as described in the case with $Re = 2 \times 10^5$ and FSTI = 10%. In this particular case, the onset of transition predicted by Eq. (18) was located right after the P8 station. Again, comparisons of the pressure coefficient distribution and the freestream velocity variation, as shown in Figs. 16a and 16b, were very good. Figures 16c and 16d showed that comparisons of the velocity profiles were good with the exception of some slight discrepancy in the last few stations.

For turbulence intensity FSTI = 2.5%, the final case was with the lowest Reynolds number, $Re = 1 \times 10^5$. The pressure coefficient and the freestream velocity distributions compared very well with the experimental data as shown in Figs. 17a and 17b, respectively. The computed velocity profiles along the suction surface were compared with the experimental data in Figs. 17c and 17d. The flow separated just before station P9 and reattached between P11 and P12 stations, resulting in a larger separation bubble when compared to the higher Reynolds number cases under the same value of FSTI. The onset of transition was located between stations P10 and P11, a position farther downstream as compared to those of the FSTI = 2.5%, $Re = 2 \times 10^5$ and 3×10^5 cases.

The turbulence kinetic energy k predicted by the current approach was reported for two cases: $Re = 1 \times 10^5$ and 2×10^5, both with FSTI = 10%. In Fig. 18, the results were compared against the measured turbulence intensity. As can be seen from Fig. 18, the freestream decay of the turbulence kinetic energy throughout the suction surface agrees very well with the experimental data. This is not surprising because the inlet conditions for the turbulence quantities were adjusted to match the decay of freestream turbulence. In

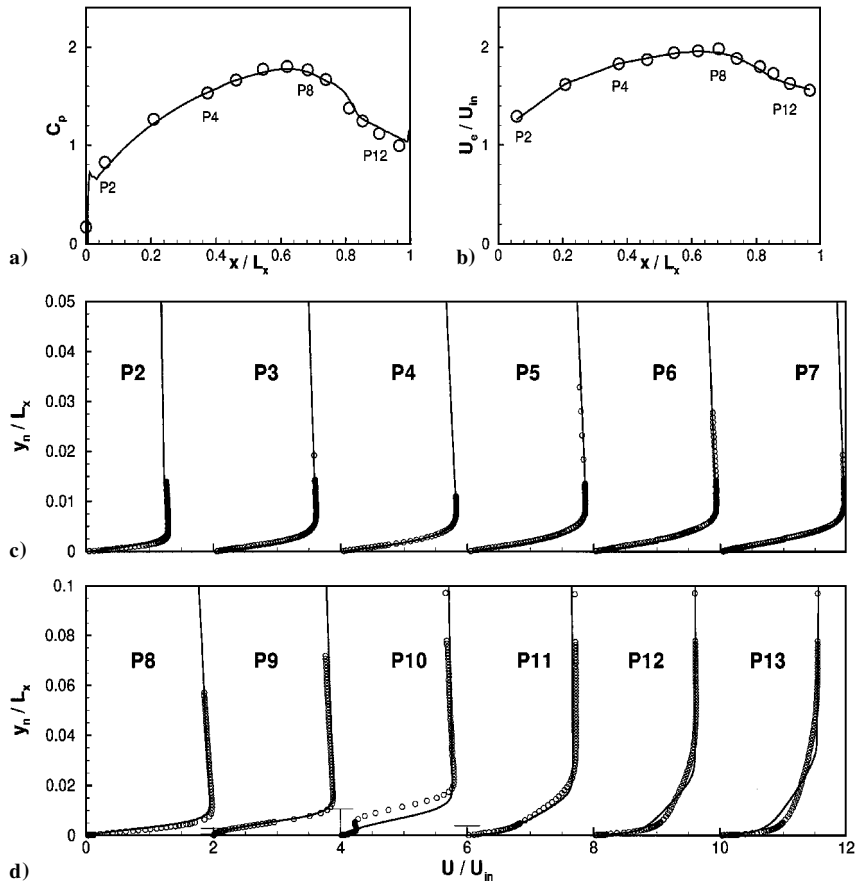

Fig. 15 Prediction of the low-pressure turbine experiment: $Re = 2 \times 10^5$ and FSTI = 2.5%.

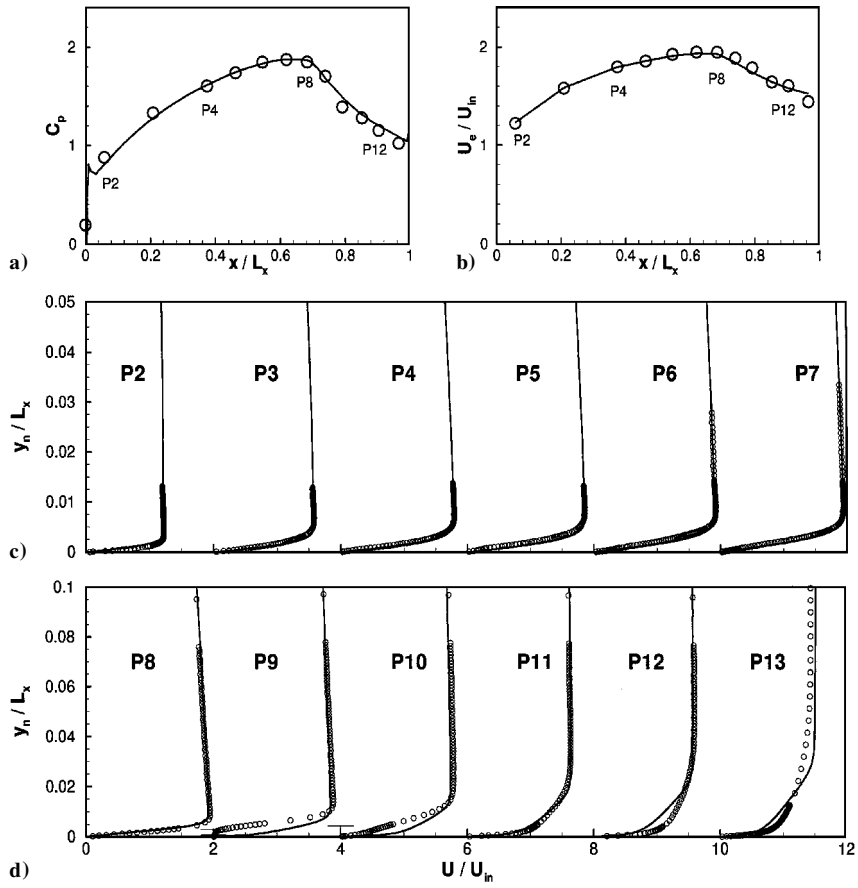

Fig. 16 Prediction of the low-pressure turbine experiment: $Re = 3 \times 10^5$ and FSTI = 2.5%.

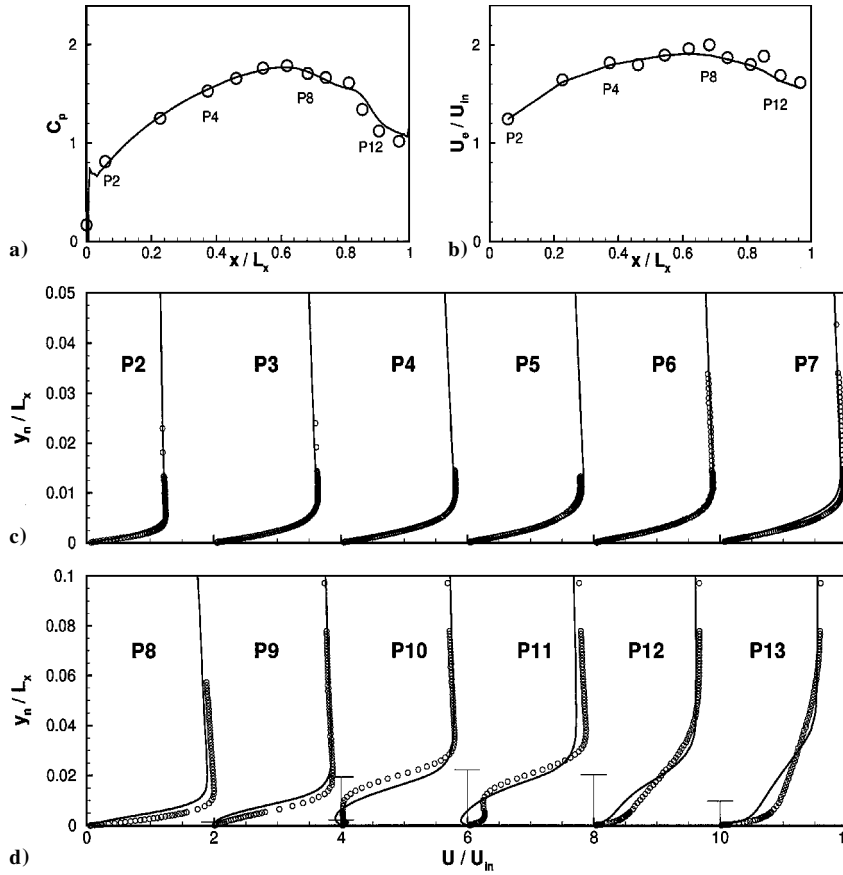

Fig. 17 Prediction of the low-pressure turbine experiment: $Re = 1 \times 10^5$ and FSTI = 2.5%.

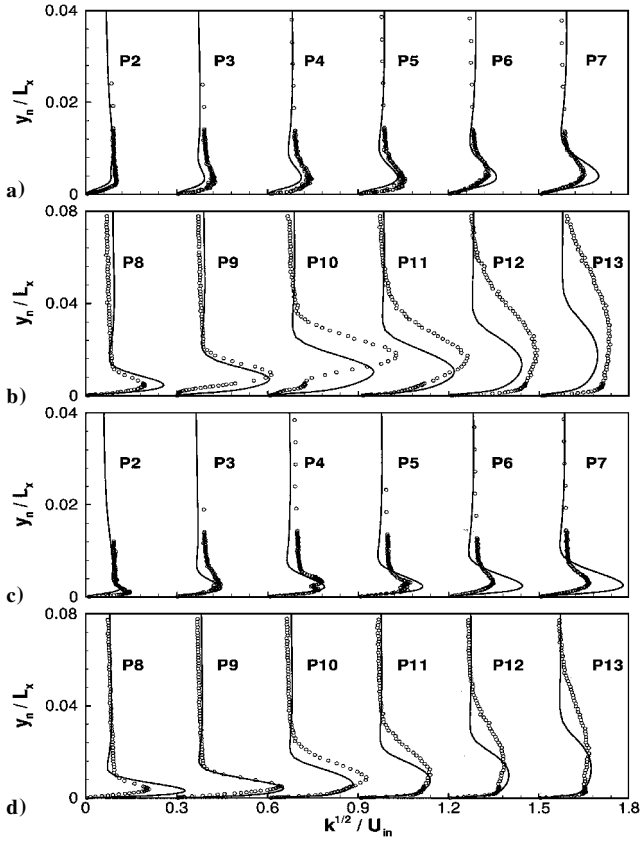

Fig. 18 Comparison of the turbulence kinetic energy: a) and b) with $Re = 1 \times 10^5$ and FSTI = 10% and c) and d) with $Re = 2 \times 10^5$ and FSTI = 10%.

general, predictions of the turbulence kinetic energy are fair. The excessive experimental values of turbulence intensity in the middle of the P10 station may be caused by the switching back and forth between laminar and turbulent flows in the intermittent region giving artificially high values of turbulence intensity.[10] Note that the measurement showed more spread of turbulence after the P11 station than the current calculation, and this feature was accompanied by fuller boundary-layer profiles in the recovery region as shown in the velocity profile comparisons (Figs. 13d and 14d). As discussed earlier, this problem may be associated with the failure of the current turbulence model to predict the flow recovery after flow reattachment.[25]

VI. Conclusions

A transport equation for the intermittency factor is employed to predict the transitional flows in low-pressure turbine applications. The intermittent behavior of the transitional flows is taken into account by modifying the eddy viscosity with the intermittency factor. The current transport model can not only reproduce the experimentally observed streamwise variation of the intermittency in the transition zone, but it also provides realistic cross-stream variation of the intermittency profile.

A comparison of the prediction and the experimental data for the T3C2 case, which has the representative pressure gradients of an aft-loaded turbine blade, has demonstrated the superiority of the current model over the pure turbulence models, namely, the k–ϵ model of Launder and Sharma,[21] the k–ω model of Wilcox,[22] and the SST model of Menter.[11] The intermittency model is further applied to predictions of a real turbine experiment of Simon et al.[10] Comparisons of surface pressure coefficients and velocity profiles show good agreement with the experimental data. Complex interactions between flow separation and transition are captured by computations. The study demonstrates the capability of the current intermittency model in predicting transitional flows in the low-pressure turbine over a range of Reynolds number and FSTI flow conditions.

Acknowledgments

This work is supported by the NASA John H. Glenn Research Center at Lewis Field under Grant NCC3-590 as part of the Low Pressure Turbine Flow Physics program. The Contract Monitor is David Ashpis.

References

[1]Savill, A. M., "Some Recent Progress in the Turbulence Modeling of By-Pass Transition," *Near-Wall Turbulent Flows*, edited by R. M. C. So, C. G. Speziale, and B. E. Launder, Elsevier, Amsterdam, 1993, pp. 829–848.

[2]Savill, A. M., "Further Progress in the Turbulence Modeling of By-Pass Transition," *Engineering Turbulence Modeling and Experiments 2*, edited by W. Rodi and F. Martelli, Elsevier, Amsterdam, 1993, pp. 583–592.

[3]Westin, K. J. A., and Henkes, R. A. W. M., "Application of Turbulence Models to Bypass Transition," *Journal of Fluids Engineering*, Vol. 119, No. 4, 1997, pp. 859–866.

[4]Libby, P. A., "On the Prediction of Intermittent Turbulent Flows," *Journal of Fluid Mechanics*, Vol. 68, Pt. 2, 1975, pp. 273–295.

[5]Steelant, J., and Dick, E., "Modelling of Bypass Transition with Conditioned Navier–Stokes Equations Coupled to an Intermittency Transport Equation," *International Journal for Numerical Methods in Fluids*, Vol. 23, No. 3, 1996, pp. 193–220.

[6]Simon, F. F., and Stephens, C. A., "Modeling of the Heat Transfer in Bypass Transitional Boundary-Layer Flows," NASA TP 3170, 1991.

[7]Dhawan, S., and Narasimha, R., "Some Properties of Boundary Layer During the Transition from Laminar to Turbulent Flow Motion," *Journal of Fluid Mechanics*, Vol. 3, Pt. 4, 1958, pp. 418–436.

[8]Huang, P. G., and Xiong, G., "Transition and Turbulence Modeling of Low-Pressure Turbine Flows," AIAA Paper 98-0339, Jan. 1998.

[9]Huang, P. G., and Coakley, T. J., "An Implicit Navier–Stokes Code for Turbulent Flow Modeling," AIAA Paper 92-0547, Jan. 1992.

[10]Simon, T. W., Qiu, S., and Yuan, K., "Measurements in a Transitional Boundary Layer Under Low-Pressure Turbine Airfoil Conditions," NASA CR 2000-209957, March 2000.

[11]Menter, F. R., "Two-Equation Eddy-Viscosity Turbulence Models for Engineering Applications," *AIAA Journal*, Vol. 32, No. 8, 1994, pp. 1598–1605.

[12]Suzen, Y. B., and Huang, P. G., "Modelling of Flow Transition Using an Intermittency Transport Equation," NASA CR 1999-209313, Sept. 1999.

[13]Suzen, Y. B., and Huang, P. G., "Modelling of Flow Transition Using an Intermittency Transport Equation," *Journal of Fluids Engineering*, Vol. 122, No. 2, 2000, pp. 273–284.

[14]Cho, J. R., and Chung, M. K., "A k–ϵ–γ Equation Turbulence Model," *Journal of Fluid Mechanics*, Vol. 237, 1992, pp. 301–322.

[15]Savill, A. M., "One-Point Closures Applied to Transition," *Turbulence and Transition Modeling*, edited by M. Hallback, D. S. Henningson, A. V. Johansson, and P. H. Alfredson, Kluwer Academic, Dordrecht, The Netherlands, 1996, pp. 233–268.

[16]Mayle, R. E., "The Role of Laminar–Turbulent Transition in Gas Turbine Engines," *Journal of Turbomachinery*, Vol. 113, No. 4, 1991, pp. 509–537.

[17]Gostelow, J. P., Blunden, A. R., and Walker, G. J., "Effects of Free-Stream Turbulence and Adverse Pressure Gradients on Boundary Layer Transition," *Journal of Turbomachinery*, Vol. 116, No. 3, 1994, pp. 392–404.

[18]Roberts, W. B., "Calculation of Laminar Separation Bubbles and Their Effect on Airfoil Performance," *AIAA Journal*, Vol. 18, No. 1, 1980, pp. 25–31.

[19]Davis, R. L., Carter, J. E., and Reshotko, E., "Analysis of Transitional Separation Bubbles on Infinite Swept Wings," *AIAA Journal*, Vol. 25, No. 3, 1987, pp. 421–428.

[20]Abu-Ghannam, B. J., and Shaw, R., "Natural Transition of Boundary Layers—The Effects of Turbulence, Pressure Gradient, and Flow History," *Journal of Mechanical Engineering Science*, Vol. 22, No. 5, 1980, pp. 213–228.

[21]Launder, B. E., and Sharma, B. I., "Application of the Energy Dissipation Model of Turbulence to the Calculation of Flow Near a Spinning Disc," *Letters in Heat and Mass Transfer,* Vol. 1, No. 2, 1974, pp. 131–138.

[22]Wilcox, D. C., "Reassessment of the Scale-Determining Equation for Advanced Turbulence Models," *AIAA Journal*, Vol. 26, No. 11, 1988, pp. 1299–1310.

[23]Sohn, K.-H., and Reshotko, E., "Experimental Study of Boundary Layer Transition with Elevated Freestream Turbulence on a Heated Flat Plate," NASA CR 187068, 1991.

[24]Gostelow, J. P., and Walker, G. J., "Similarity Behavior in Transitional Boundary Layers over a Range of Adverse Pressure Gradients and Turbulence Levels," *Journal of Turbomachinery*, Vol. 113, No. 4, 1991, pp. 617–625.

[25]Huang, P. G., "Physics and Computation of Flows Under Adverse Pressure Gradients," *Modeling Complex Turbulent Flows*, ICASE/LaRC Interdisciplinary Series in Science and Engineering, edited by M. D. Salas, J. N. Hefner, and L. Sakell, Kluwer Academic, Dordrecht, The Netherlands, 1999, pp. 245–258.

[26]Huang, P. G., and Coakley, T. J., "Turbulence Modeling for Complex Hypersonic Flows," AIAA Paper 93-0200, Jan. 1993.

[27]Huang, P. G., "Validation of Turbulence Models—Uncertainties and Measures to Reduce Them," American Society of Mechanical Engineers, ASME Paper 97-3121, 1997.

P. Givi
Associate Editor